Article

Not peer-reviewed version

Preparation of pH-Responsive PET TeMs by Controlled Graft Block Copolymerisation of Styrene and Methacrylic Acid for the Separation of Water-Oil Emulsions

Indira B. Muslimova *, Dias D. Omertassov, Nurdaulet Zhumanazar, Nazerke Assan, Zhanna K. Zhatkanbayeva, Ilya V. Korolkov *

Posted Date: 30 June 2025

doi: 10.20944/preprints202506.2325.v1

Keywords: pH-responsive membranes; track-etched membranes; RAFT graft polymerization; separation; antifouling; poly(ethylene terephthalate)

 doi:10.20944/preprints202506.2325.v1

Article

Preparation of pH-Responsive PET TeMs by Controlled Graft Block Copolymerisation of Styrene and Methacrylic Acid for the Separation of Water-Oil Emulsions

Indira B. Muslimova [1,2,*], Dias D. Omertassov [1,2], Nurdaulet Zhumanazar [1], Nazerke Assan [2], Zhanna K. Zhatkanbayeva [2] and Ilya V. Korolkov [1,2,*]

[1] The Institute of Nuclear Physics, 050032, Ibragimov str. 1, Almaty, Kazakhstan

[2] L.N. Gumilyov Eurasian National University, Satpaev Str., 2, Astana 010000, Kazakhstan

* Correspondence: i.korolkov@inp.kz (I.V.K.); i.muslimova@inp.kz (I.M.B.)

Abstract

To develop membranes capable of efficient and switchable separation of emulsions under variable pH conditions, pH-responsive surfaces were engineered by modifying poly(ethylene terephthalate) track-etched membranes (PET TeMs) via a two-step UV-initiated RAFT graft polymerization. Initially, polystyrene (PS) was grafted to render the surface hydrophobic, followed by the grafting of poly(methacrylic acid) (PMAA) to introduce pH-responsive carboxyl groups. Optimized conditions (117 mM MAA, RAFT:initiator 1:10, 60 min UV exposure at 10 cm) resulted in PET TeMs-g-PS-g-PMAA surfaces exhibiting tunable wettability, with contact angles shifting from 90° at pH 2 to 65° at pH 9. Successful grafting was confirmed by FTIR, AFM, SEM, TGA, and TB dye sorption. The membranes showed high separation efficiency (up to 99%) for both direct and reverse emulsions. In direct emulsions, stable flux values (70 to 60 L m^{-2} h^{-1} for cetane-in-water and 195 to 120 L m^{-2} h^{-1} for o-xylene-in-water) were maintained over five cycles at 900 mbar, indicating good antifouling behavior. Reverse emulsions exhibited initially higher flux, but stronger fouling; however, flux recovery reached 91% after cleaning. These findings demonstrate the potential of PET TeMs-g-PS-g-PMAA as switchable, pH-responsive membranes for robust emulsion separation.

Keywords: pH-responsive membranes; track-etched membranes; RAFT graft polymerization; separation; antifouling; poly(ethylene terephthalate)

1. Introduction

The evolution of membrane technologies has shifted from traditional passive filtration systems to the development of adaptive, multifunctional platforms capable of responding dynamically to external stimuli[1–3]. This transition is particularly evident in fields such as biomedicine, environmental protection, and industrial filtration, where membrane functionality must extend beyond simple selective separation, in particular for the separation of water-oil emulsions (WOE). Stimuli-responsive membranes, designed to alter their surface properties under external triggers such as pH, temperature, ionic strength, or light, have gained increasing attention for their ability to enhance selectivity, fouling resistance, and operational flexibility[4–6].

Track-etched membranes (TeMs), based on poly(ethylene terephthalate) (PET), offer an ideal substrate for the development of such intelligent systems due to their well-defined pore geometry, mechanical robustness, and chemical stability[7–9]. Recent advances in controlled polymerization techniques, such as reversible addition-fragmentation chain transfer (RAFT) polymerization, have enabled the precise modification of membrane surfaces, allowing the creation of tailored wettability

 doi:10.20944/preprints202506.2325.v1

and switchable separation behavior[10,11]. By grafting functional polymers onto PET TeMs, it is possible to impart dynamic surface characteristics[12–15].

While conventional PET TeMs primarily enable efficient size-selective filtration[16], current research increasingly emphasizes surface functionality. In particular, strategies have been developed to produce membranes with entirely hydrophilic or hydrophobic surfaces. Radiation-induced grafting of acrylic acid (AA) has been shown to enhance hydrophilicity without compromising mechanical strength, extending usability in filtration, separation, and biomedical applications[17]. Incorporation of poly(1-vinyl-2-pyrrolidone) enables metal nanoparticle immobilization for use in catalytic degradation of pollutants such as metronidazole[18], while grafting of poly(*N*-isopropylacrylamide) via atom transfer radical polymerization (ATRP) introduces temperature-responsiveness[19]. Membranes grafted with AA demonstrate high selectivity for alkaline ions (Li^+, K^+, Na^+), valuable for dialysis and ion exchange[20]. On the hydrophobic side, modification with fluorinated monomers like dodecafluoroheptyl acrylate or heptafluorobutyl methacrylate yields superhydrophobic membranes (CA > 97°), suitable for membrane distillation and oil-water separation[21,22]. Additionally, the immobilization of hydrophobic vinyl-silica nanoparticles significantly improves water flux and salt rejection in direct contact membrane distillation[23]. The use of lauryl and stearyl methacrylates further enhances oil selectivity, and fluorosilane-based nanoparticles improve antifouling characteristics[24,25]. Thus, targeted functionalization strategies have significantly advanced membranes to selectively interact with specific chemical species or to perform under demanding physical conditions. Nevertheless, in dynamic environments—especially in the treatment of WOE there remains a growing demand for materials that can reversibly adapt their surface properties.

Among various stimuli-responsive approaches, pH-switchable systems are particularly attractive due to the ease of controlling pH and the availability of polymers with well-defined ionization behavior. Incorporating pH-responsive polymer layers onto PET TeMs expands their applicability to systems where the controlled wettability is required. This responsiveness enables selective permeability, improved antifouling behavior, and potential for self-cleaning under cyclic operation. A range of pH-responsive polymers have been employed either as individual components or as part of copolymers in the fabrication of smart membranes designed for WOE separation [1,2,26–28]. Poly(acrylic acid) (PAA) and poly(methacrylic acid) (PMAA) are among the most commonly used anionic pH-sensitive polymers. Their carboxyl groups ionize in alkaline media, enhancing membrane hydrophilicity. Membranes grafted with PAA or PMAA typically exhibit separation efficiencies above 90% and maintain fluxes ranging from 1000 to 4000 L m^{-2} h^{-1} depending on emulsion type and structure[29–31]. Poly(4-vinylpyridine) (P4VP) offers a basic nitrogen functionality that protonates under acidic conditions, making membranes hydrophilic at low pH[32]. PET-based TeMs grafted with P4VP demonstrated CA variations from 95° (pH 9) to 52° (pH 2), with stable separation efficiencies between 95–100% and fluxes to 7000 L m^{-2} h^{-1} over multiple cycles[33]. Poly(2-(dimethylamino)ethyl methacrylate) (PDMAEMA) and related tertiary amine-containing methacrylates are also used due to their tunable pKa values (~7.3), contributing to superhydrophilic or oleophobic states under mildly acidic or basic conditions. These materials enable flux rates up to 5000 $L \cdot m^{-2} \cdot h^{-1}$ and separation efficiencies exceeding 63-99%[34–36]. The addition of nanostructures such as SiO_2 or TiO_2 can further enhance surface roughness and responsiveness, improving both selectivity and antifouling characteristics under varying pH.

Building on this foundation, PET-based TeMs emerge as especially favorable substrates for creating pH-responsive forms, above their narrow pore size distribution, mechanical robustness, and chemical inertness for acids. Their suitability for graft polymerization enables precise surface functionalization without compromising pore structure integrity[37].

In this study, we employed a two-step UV-initiated RAFT graft polymerization strategy to fabricate pH-responsive PET TeMs. In the first step, a stable hydrophobic polystyrene (PS) layer was grafted onto PET TeMs. In the second, PMAA was grafted onto the PS chains, introducing pH-

 doi:10.20944/preprints202506.2325.v1

sensitive carboxyl groups. This approach allowed controlled grafting while preserving the porosity of the membrane and giving it an adjustable wettability.

The main objectives of this work were to optimize the second-stage grafting conditions, to characterize the physicochemical properties of the modified membranes via FTIR-ATR, SEM, AFM, TGA, and dye toluidine blue (TB) sorption, and to assess membrane performance in the separation of both direct and reverse water-oil emulsions. Special attention was paid to evaluating flux, antifouling properties and flux recovery during multiple filtration cycles, thereby demonstrating the potential of PET TeMs-g-PS-g-PMAA membranes as versatile, responsive platforms for emulsion treatment under variable pH conditions.

2. Materials and Methods

2.1. Materials and Chemicals

Membrane base: Poly(ethylene terephthalate) track-etched membranes (PET TeMs), Mitsubishi Polyester Film. Monomers: Styrene (ST) and methacrylic acid (MAA), Sigma-Aldrich. RAFT agent: 2-(Dodecylthiocarbonothioylthio)-2-methylpropionic acid, Sigma-Aldrich. Photoinitiator: Benzophenone (BP), Sigma-Aldrich. Solvents and other chemicals: N,N-Dimethylformamide (DMF), isopropyl alcohol (IPA), chloroform, benzene, o-xylene, sodium hydroxide, and hydrochloric acid, all with analytical grade purity of ≥95%. Deionized water (18.2 MΩ) was prepared using the Akvilon-D 301. UV lamps: OSRAM Ultra Vitalux E27 (315-400 nm, 13.6 W) was used in grafting, and Osram Puritec (254 nm,12 W) was used in photosensitization. Other materials: polyvinyl chloride (PVC) film and filtration set, ISOLAB Laborgeraete GmbH; Ultra-Turrax disperser and Vacstar control pump, IKA.

2.2. Preparation and Modification of Track-Etched Membranes

Figure 1 shows a schematic of the stepwise preparation of pH-sensitive membranes from PET film. This technique was developed on the basis of previous studies on modification of PET TeMs[25,30,33,38] and optimized to obtain membranes with switchable surface hydrophobicity/hydrophilicity for the separation of water-in-oil/oil-in-water emulsions by changing the pH-medium.

2.2.1. Track-Etched Membranes Base Preparation: Irradiation and Etching of PET Films

The production of TeMs was carried out using 23 μm thick poly(ethylene terephthalate) films. These films were subjected to irradiation at the DC-60 cyclotron in Astana, Kazakhstan, employing Kr ions at an energy level of 1.75 MeV per nucleon, achieving a latent track density of approximately 1 × 10^6 ions/cm². Following irradiation, the films underwent a photosensitization phase under UV light with a 254 nm wavelength, applied from a distance of 10 cm for 30 minutes on each side. Photosensitization stimulates photooxidation of damaged areas of the irradiated PET film, thereby increasing the chemical track-etching rate, which is significantly slower under normal conditions. Chemical etching was carried out in a solution of 2.2 M sodium hydroxide at an elevated temperature of 85 °C for 10-12 min. As a result of alkaline hydrolysis, the PET ester bonds (—C(=O)O—) were broken and carboxyl (-COOH) and hydroxyl (-OH) groups were formed on the film surface, and pores with a diameter of about 2.33 ± 0.07 μm were formed in place of the damaged areas. After etching, the PET TeMs were washed in 3% acetic acid solution and in distilled water to neutralize the alkali residue and wash off the hydrolysis products.

2.2.2. UV-Initiated RAFT Graft Polymerization for PET TeMs Modification

The membrane modification was performed by UV-initiated grafting RAFT polymerization using benzophenone (BP) as a UV initiator, 2-(Dodecylthiocarbonothioylthio)-2-methylpropionic acid as a RAFT agent, styrene (ST) and methacrylic acid (MAA) as monomers, and isopropyl alcohol

 doi:10.20944/preprints202506.2325.v1

(IPA) as a solvent. Modification of PET TeMs was performed under a UV lamp with a wavelength of 315–400 nm at a power of 13.6 W in an argon atmosphere. To activate the surface, PET TeMs was kept in a 5% BP solution in dimethylformamide (DMF) for 24 hours without access to light.

Immediately before UV grafting, PET TeMs was washed in DMF to remove excess BP. Then, the PET TeMs was immersed in a container with a reaction mixture of the first monomer - ST. The carboxyl and hydroxyl groups formed after chemical etching, the adsorbed BP on the membrane surface, and the RAFT agent with BP in the reaction mixture ensured uniform grafting of the polymer layer. The grafting of polystyrene (PS) was carried out according to the optimal parameters found in early research[33]: the concentration of PS in the reaction mixture was 172 mM, the molar ratio of the RAFT agent: initiator in the reaction mixture was 1:10, the distance from the UV source was 7.5 cm, and the UV irradiation time was 60 min. The grafted PS layer, with DG_{PS} 2.5-2.7%, provides stable hydrophobicity on the surface of PET TeMs-g-PS with a CA 98±3°, whereas unmodified PET TeMs are moderately hydrophilic, with a CA 60°. The pore structure of the hydrophobic PET TeMs-g-PS is preserved, with a slight decrease in pore diameter from 2.33±0.07 to 2.14±0.1 μm.

In the second step, a similar procedure was used for grafting MAA onto the surface of PET TeMs-g-PS with optimization of the parameters for controlled wettability. The concentration of methacrylic acid was varied from 30 to 350 mM, the molar ratio of the RAFT agent:initiator was from 1:1 to 1:30, the distance from the UV source was from 7.5 to 15 cm, and the UV irradiation time was from 30 to 60 min. Grafting of poly(methacrylic acid) (PMAA) was achieved by activating the dormant radical of the RAFT agent at the ends of the TeMs-g-PS PET chains, which ensured controlled growth of the second block[39–41]. The selection of optimal parameters for grafting pH-sensitive PET TeMs-g-PS-g-PMAA was carried out based on the response of the CA of their surface to changes in the acidity of the medium at pH 2 and pH 9.

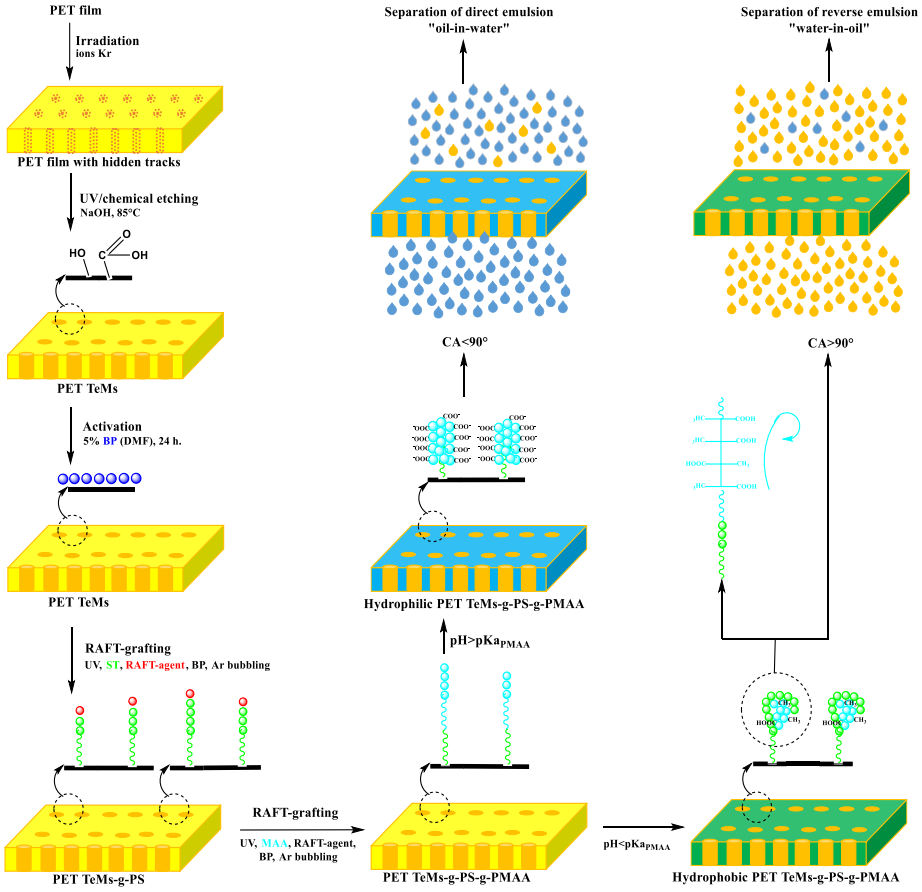

 doi:10.20944/preprints202506.2325.v1

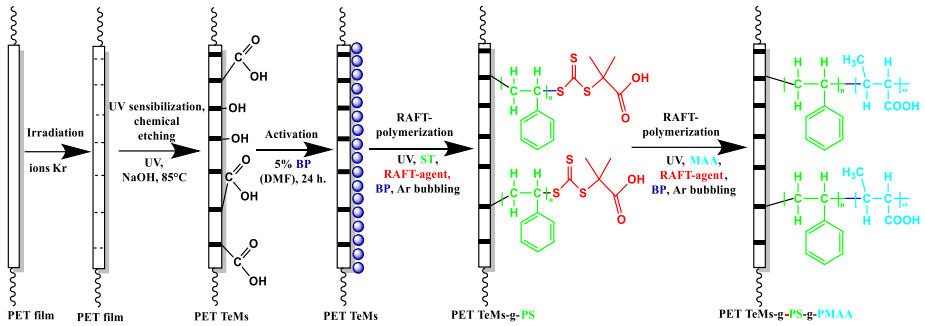

Figure 1. Scheme for the preparation of pH-responsive PET TeMs-g-PS-g-PMAA for the separation of water-oil emulsions.

2.3. PET TeMs-g-PS-g-PMAA characterization

2.3.1. Contact Angle (CA) Measurement and pH-Responsivity Evaluation

CA of the membrane surface with liquids was measured at six different positions on the sample using a digital microscope with 1000x magnification, employing the static drop method at room temperature. The surface free energy (ω, mN/m) and its polar component (γ_p, mN/m) were calculated by the Owens, Wendt, Rabel, and Kelble method using diiodomethane as a non-polar liquid. The pH-responsivity of PET TeMs-g-PS-g-PMAA was evaluated by measuring the CA response under different pH conditions to identify the optimal grafting parameters of PMAA that result in the most pronounced transition in wettability between hydrophilicity and hydrophobicity.

The transition in wettability was observed at pH values below and above the $pKa_{(PMAA)}$ 4.8. Figure 1 visualizes the controlled transition of membrane surface wettability in response to a change in pH. The membranes were immersed in solutions with pH values of 2 and 9 for 30 minutes, after which the CA was measured.

2.3.2. Degree of Grafting (DG) Determination

The degree of grafting (DG, %) was calculated by measuring the weight of the membranes before and after the grafting process, according to the following equation (1):

$$DG = (m_2 - m_1)/m_1 \times 100\% \quad (1)$$

where m_1 — is the mass of the membrane before grafting, and m_2 — is the mass of the membrane after grafting.

2.3.3. Atomic Force Microscopy (AFM)

AFM on an NT-206 device (ALC Microtestmachines, Belarus) was used to evaluate the surface morphology of the modified membranes. The parameters of average roughness (Ra, nm) and root-mean-square roughness (Rq, nm), as well as local mechanical properties such as adhesion force (Fa, nN) and elastic modulus (E, MPa) were studied. Measurements were carried out in five scanning zones (4×4 μm) with subsequent data processing in the Surface Explorer software.

2.3.4. UV-Vis Spectroscopy

A Specord-250 UV-vis spectrophotometer (Analytik Jena, Germany) was used to analyze the presence of carboxyl groups on the membrane surface before and after modification. The concentration of carboxyl groups was determined based on the sorption of toluidine blue (TB) dye followed by measurement of its desorption at a wavelength of 633 nm.

2.3.5. Thermogravimetric Analysis (TGA)

 doi:10.20944/preprints202506.2325.v1

TGA was performed on a Pyris 1 TGA device (PerkinElmer, USA) in the temperature range from 0 to 700 °C at a heating rate of 10 °C/min under nitrogen atmosphere to study the thermal stability of the membranes and to determine the decomposition temperatures and composition of PET TeMs-g-PS-g-PMAA polymer layers.

2.3.6. Fourier Transform Infrared Spectroscopy (FTIR)

FTIR spectra were recorded on an InfraLUM FT-08 spectrometer (Lumex, Russia) using an ATR attachment to analyze the chemical structure of the membranes and to confirm the presence of functional groups introduced during the grafting process. A resolution of 2 cm^{-1} with a minimum number of scans of 20 was used for the analysis. The spectra were processed using the SpectraLUM® software suite. Peak intensities were normalized relative to reference peaks at 1409 and 1245 cm^{-1}, which correspond to phenyl ring vibrations (C–H bending coupled with ring stretching) and the asymmetric stretching vibration of C(=O)–O, respectively.

2.3.7. Scanning Electron Microscopy (SEM)

SEM was used to investigate the surface morphology of the membranes and to monitor pore diameter on a Hitachi TM 3030 instrument (Hitachi, Japan).

2.4. Performance Assessment of PET TeMs-g-PS-g-PMAA in Water-Oil Emulsion Separation

The performance of membranes with an area of 0.001256 m^2 was tested in the filtration unit that was employed in previous studies. Vacuum pressure of 900, 700 and 500 mbar was maintained using a Vacstar Control Pump. Depending on the emulsion type, the membranes were soaked for 30 minutes in water at pH 2 for reverse emulsions and at pH 9 for direct emulsions (Figure 1). The emulsions were prepared by mixing oil and water components at a volume ratio of 1:100 using an Ultra-Turrax at 24,000 rpm for 1 minute. The oil components included o-xylene, chloroform, and cetane. Water at pH 2 was used as the dispersed component for reverse emulsions, while water at pH 9 was used as the external component for direct emulsions.

Membrane performance was evaluated by calculating the flux of the filtered liquid using equation (2), and the separation rate was determined using equation (3), as outlined in previous works[25,30,33,38,42]:

$$F = V/(S \times t) \quad (2)$$

$$R = (V_2/V_1) \times 100\% \quad (3)$$

where F—is the flux, L m^{-2} h^{-1}; V—is the volume of external component that permeates through the membrane, L; S—is the filtration area of PET TeMs-g-PS-g-PMAA, m^2; and t—is the flow time, h; R—is the separation rate, V_1—is the volume of dispersed component before separation; and V_2—is the volume of dispersed component after separation.

2.4.1. Evaluation of PET TeMs-g-PS-g-PMAA Fouling and Flux Recovery in Water-Oil Separation

Membrane fouling and rejection performance were evaluated by calculating the flux recovery and total flux reduction factor according to equations (4) and (5)[30,42]:

$$FR = (F_2/F_1) \times 100\% \quad (4)$$

$$TR = (1 - (F_0/F_1)) \times 100\% \quad (5)$$

 doi:10.20944/preprints202506.2325.v1

where FR — is the flux recovery, %; TR — is the total flux reduction factor, %; F_1, F_2 — fluxes of external components determined before and after emulsion separation, L m^{-2} h^{-1}; F_0 — emulsion separation flux, L m^{-2} h^{-1}.

The pure external component flux was measured during reverse emulsion separations of chloroform, cetane, and o-xylene, as well as during direct emulsion separations with water at pH 9. After each separation, the membranes were cleaned by soaking in a pH 2 solution for reverse emulsions and in a pH 9 solution for direct emulsions. The flux of the external component was then measured again.

3. Results and Discussions

This section may be divided by subheadings. It should provide a concise and precise description of the experimental results, their interpretation, as well as the experimental conclusions that can be drawn.

PET TeMs-g-PS with a stable hydrophobic layer (DG_{PS} of 2.6±0.1%, CA of 98±3°, pore diameter of 2.33±0.07 μm) were used as a substrate for UV-initiated RAFT graft polymerization of PMAA to create pH-responsive membranes. As shown in Figure 1, the Z-group (-$SC(CH_3)_2COOH$) of RAFT-agent, which "sleeps" at the PS chain ends, activates the grafting of PMAA to PS-g-PET TeMs. The reaction pathways for the formation of block copolymer on the surface of PET TeMs are well described in an earlier work[30].

Figure 2 presents the changes in DG_{PMAA} and CA of the PET TeMs-g-PS-PMAA surface under varying polymerization conditions. Increasing the grafting time from 30 to 75 minutes, raising the MAA concentration from 30 to 350 mM, and reducing the distance to the UV source from 15 to 7.5 cm result in an increase in DG_{PMAA} from 0 to 3.48±0.22%. The closer proximity to the UV source enhances the UV intensity, thereby increasing the rate of radical formation. Extending the grafting time promotes higher monomer conversion and the growth of longer PMAA chains, while a higher MAA concentration in the reaction mixture facilitates more efficient polymerization. Collectively, these factors contribute to an increase in PMAA grafting density on the PET TeMs surface. This, in turn, leads to a higher concentration of carboxyl functional groups, increasing the hydrophilicity of the membranes, as indicated by a decrease in CA from 98° to 52° at pH 2. At pH 9, even membranes with a minimal DG_{PMAA} of 0.1% exhibit hydrophilicity with CA <90°. These trends are consistent with previous studies [43,44], which also reported a correlation between the quantification of DG_{PMAA}, CA, and polymerization conditions of hydrophilic monomers.

Increasing the molar ratio of the RAFT agent to the initiator from 1:1 to 1:30 in the reaction mixture causes a decrease in the DG_{PMAA} from 0.5 to 2.5±0.4% (Figure 2b). This trend is attributed to the quantitative predominance of the initiator, which diminishes the control exerted by the RAFT agent and promotes the formation of PMAA homopolymer rather than grafted polymer chains on the PET TeMs surface. Furthermore, the pH responsivity of these membranes, as determined by contact angle (CA) measurements (Figure 2b), changes by only 6–12° when the pH is varied from 2 to 9, suggesting uncontrolled polymerization and premature chain termination. Under such conditions, a broader molecular weight distribution leads to an uneven distribution of pH-sensitive functional groups, thereby attenuating the overall pH response[45,46].

FTIR-ATR spectra (Figure 3) of the membranes before and after grafting consist of characteristic PET TeMs-g-PS absorption peaks and they agree on wave numbers in articles[47,48]: absorption peaks of PET TeMs: for the ester C=O groups 1712 cm^{-1}, for aromatic ring bending CH 1409 cm^{-1}, bending CCC 1017 cm^{-1}, stretching CC 872 cm^{-1}, for bending CH_2 groups 1340 cm^{-1}, for stretching C(=O)-O groups 1245 cm^{-1}, for stretching C-O groups 971 cm^{-1}; absorption peaks of PS: for bending C-H out- of-plane 700 cm^{-1} and 760 cm^{-1}, for stretch ring C=C aromatic 1601 cm^{-1}, 1492 cm^{-1} and 1452 cm^{-1}. After PMAA grafting, notable spectral changes appear, as clearly seen in Figure 3b, with the emergence of absorption bands at 2852 cm^{-1} and 2925 cm^{-1} corresponding to the aliphatic C-H vibrations of PMAA. The carboxyl (-COOH) and hydroxyl (-OH) groups characteristic of PMAA are not distinctly registered in the FTIR spectra due to their relatively low concentration. However, the

 doi:10.20944/preprints202506.2325.v1

sorption of TB dye confirms the presence of terminal -COOH groups on the PET TeMs-g-PS-g-PMAA surface. As the DG_{PMAA} increases from 0.1 to 3.48±0.22%, COOH groups concentration slightly rises from 0.95 to 1.16 mmol/L (0.8 mmol/L for PET TeMs-g-PS[30]).

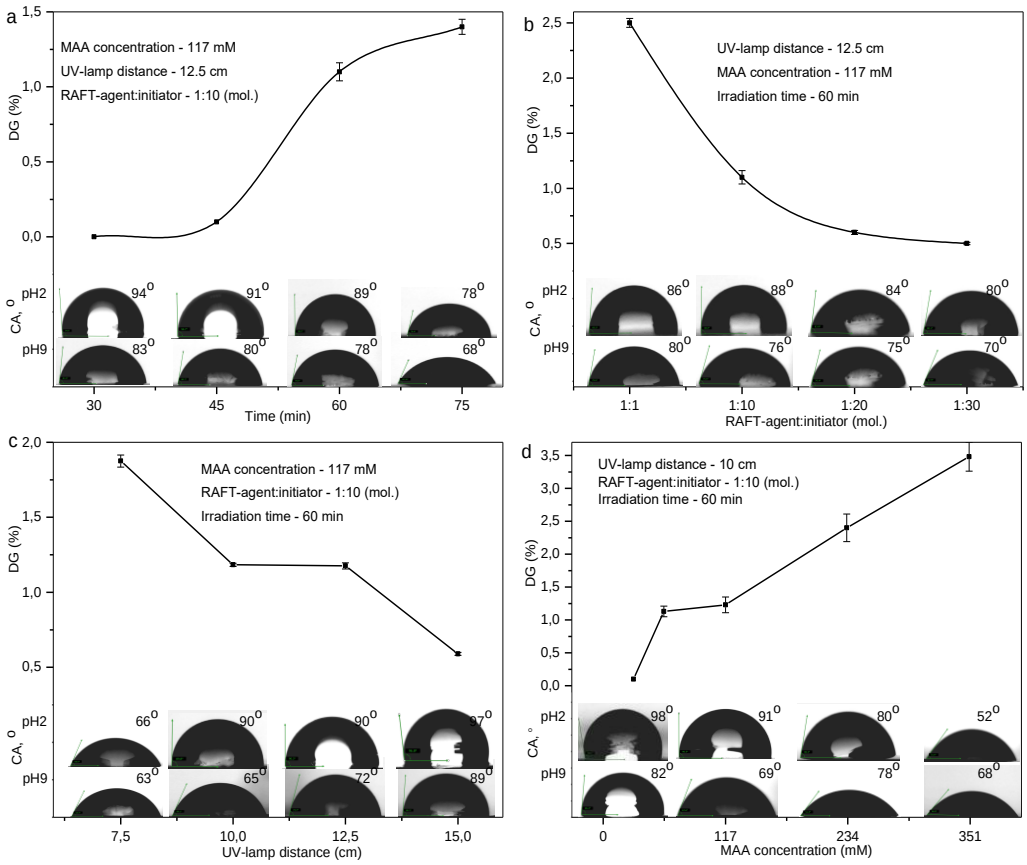

Figure 2. CA at pH 2 and pH 9 and corresponding DG_{PMAA} for PET TeMs-g-PS-g-PMAA obtained under different UV-initiated RAFT graft polymerization conditions: time (a), molar ratio of RAFT-agent:initiator (b), distance from UV-lamp (c) and concentration of MAA (d).

A more detailed analysis of the FTIR peak ratios is presented in Table 1 and shows that as the molar ratio of the RAFT-agent to the initiator increases from 1:1 to 1:30, the intensity ratios I_{1712}/I_{1409} and I_{1712}/I_{1245} decrease from 5.00 to 4.00 and from 0.91 to 0.82, respectively, indicating a reduction in the number of carboxyl (-COOH) groups. Simultaneously, the intensity ratios I_{2850}/I_{1409} and I_{2925}/I_{1409} increase from 0.17 to 0.43 and from 0.33 to 0.57, respectively, which is consistent with the formation of a more branched polymer architecture and hindered packing of polymer chains. These findings confirm that an excess of initiator leads to uncontrolled polymerization, reducing grafting efficiency, decreasing the number of available -COOH sites, and consequently resulting in decreased pH-responsivity of the membranes.

 doi:10.20944/preprints202506.2325.v1

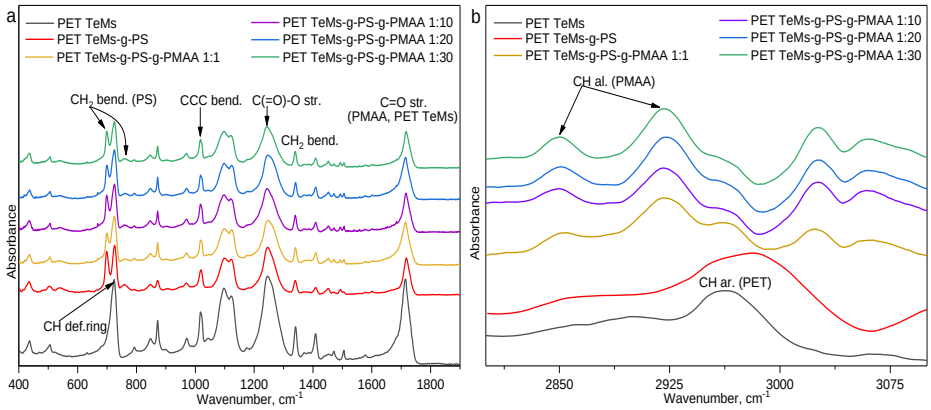

Figure 3. FTIR-ATR spectra of PET TeMs, PET TeMs-g-PS, and PET TeMs-g-PS-g-PMAA obtained at different RAFT agent:initiator molar ratios: in the range 400-1800 cm^{-1} (a) and range 2800-3100 cm^{-1} (b).

Table 1. Intensity ratios of FTIR-ATR absorption bands for PET TeMs, PET TeMs-g-PS, and PET TeMs-g-PS-g-PMAA obtained at different RAFT agent:initiator molar ratios.

Sample	I_{2850}/I_{1409}	I_{2850}/I_{1245}	I_{2925}/I_{1409}	I_{2925}/I_{1245}	I_{1712}/I_{1409}	I_{1712}/I_{1245}
PET TeMs	-	-	-	-	4.91	0.93
PET TeMs-g-PS	-	-	-	-	1.67	0.31
PET TeMs-g-PS-g-PMAA RAFT agent:initiator 1:1, DG_{PMAA}=2.5%	0.17	0.03	0.33	0.06	5.00	0.91
PET TeMs-g-PS-g-PMAA RAFT agent:initiator 1:10, DG_{PMAA}=1.1%	0.20	0.03	0.40	0.06	5.40	0.84
PET TeMs-g-PS-g-PMAA RAFT agent:initiator 1:20, DG_{PMAA}=0.6%	0.18	0.03	0.35	0.06	4.83	0.88
PET TeMs-g-PS-g-PMAA RAFT agent:initiator 1:30, DG_{PMAA}=0.5%	0.43	0.09	0.57	0.12	4.00	0.82

Based on the obtained AFM images (Figure 4), as the irradiation time increases from 30 to 75 min, the grafting of PMAA onto the PET TeMs-g-PS surface (Ra = 8.4±0.9 nm, Rq = 12±2.1 nm, E = 126±10 MPa, Fa = 63±5 nN) leads to the formation of surface irregularities, making the morphology more pronounced and complex. The Ra and Rq values increase to 17±0.1 and 24±1.3 nm, respectively, while the mechanical resistance to deformation increases, as evidenced by an increase in the E to 155±10 MPa.

 doi:10.20944/preprints202506.2325.v1

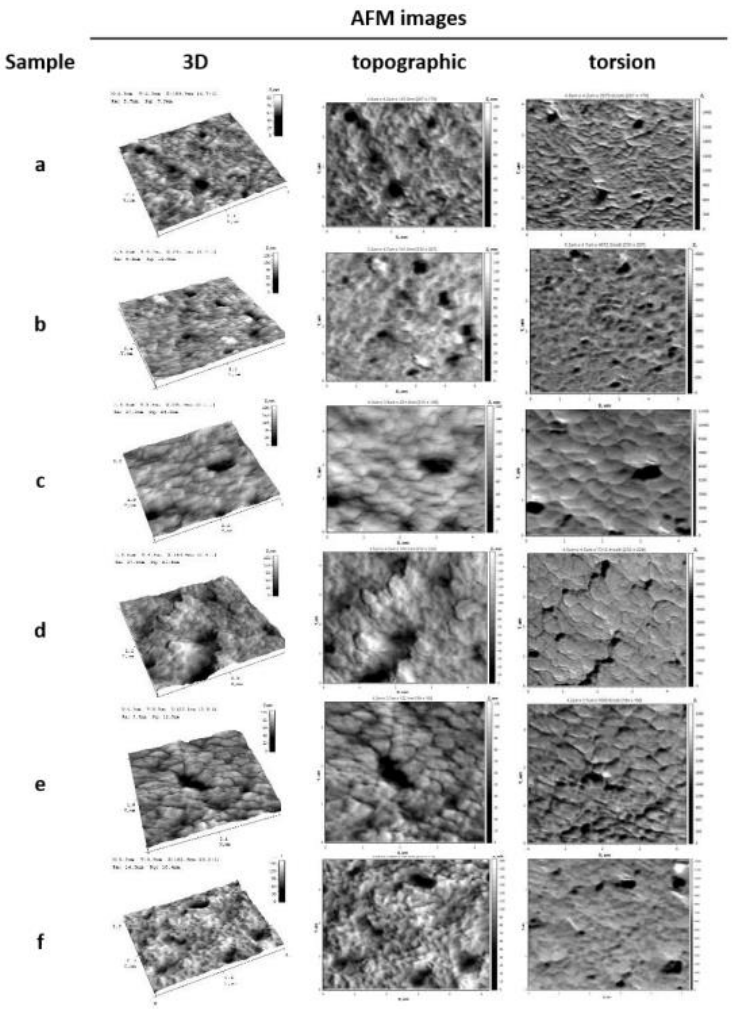

Figure 4. 3D, topographic, and torsion AFM images and basic surface characteristics of PET TeMs (a), PET TeMs-g-PS (b), and PET TeMs-g-PS-g-PMAA obtained by different irradiation times: 30 min (c), 45 min (d), 60 min (e), and 75 min (f). All samples were prepared with a constant PMAA concentration of 117 mM, RAFT agent:initiator molar ratio of 1:10, and a UV-source distance of 10 cm.

Significant changes in interfacial adhesion between the PMAA layer and the substrate are observed: the Fa value increases for samples grafted for 30 and 75 minutes to 91 and 112±5 nN, respectively. However, for samples irradiated for 60 minutes, Fa decreases to 31±5 nN and fluctuates within the measurement error at 62±5 nN for samples grafted for 45 minutes.

SEM images before and after PMAA grafting are presented in Figure 5. As DG_{PMAA} increases, the surface morphology becomes smoother at the microscale. A decrease in the distance between the UV source and the sample from 15 to 7.5 cm results in a reduction in pore diameter from 2.09±0.08 μm to 1.90±0.08 μm due to denser PMAA grafting (DG_{PMAA} increases from 0.59±0.01% to 1.87±0.04%) onto the PET TeMs-g-PS surface (initial pore diameter 2.14±0.16 μm).

 doi:10.20944/preprints202506.2325.v1

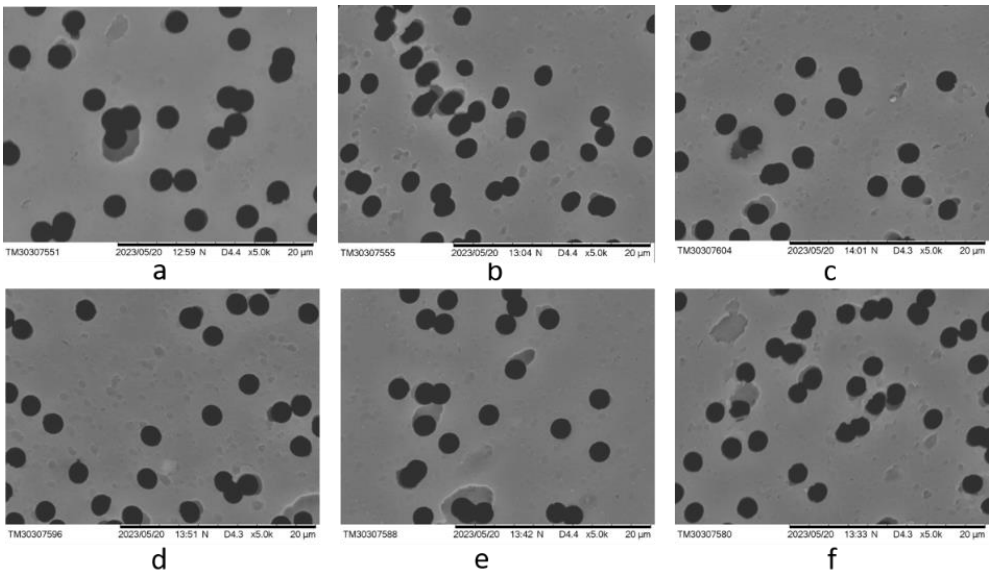

Figure 5. SEM images of PET TeMs (a), PET TeMs-g-PS (b), and PET TeMs-g-PS-g-PMAA obtained at different distances from the UV-source: 15 cm(c), 12.5 cm (d), 10 cm (e), and 7.5 cm(f). All samples were prepared with a constant PMAA concentration of 117 mM, RAFT agent-to-initiator molar ratio of 1:10, and an irradiation time 60 min.

TGA and DTG curves for PET TeMs-g-PS-g-PMAA membranes are shown in Figure 6. The thermogram of the pristine PET TeMs exhibits a single-phase decomposition process characteristic of the main PET polymer backbone. Decomposition starts at 382°C, with the maximum degradation rate observed at 463°C. PS grafting leads to a slight reduction in thermal stability, with the decomposition temperature remaining close to that of the
pristine PET TeMs. The data for PET TeMs-g-PS are consistent with earlier work[30]. PMAA grafting results in more significant changes: the first peak at 123°C, with a 1% mass loss, indicates a physical evaporation process, as hydrophilic PMAA side groups can retain water or small amounts of volatile compounds, such as the IPS solvent. The main decomposition process shifts to 452°C, with a mass loss of 51%, indicating PMAA chain degradation.

Thus, PS and PMAA grafting is confirmed by thermogravimetric analysis, demonstrating trends similar to those observed with PAA, but with a more pronounced shift in decomposition temperatures and greater mass loss. Additional degradation peaks at 521°C and 630°C, with mass losses of 16% and 10%, respectively, may be associated with further thermal degradation of membrane residues.

As a result of this study, pH-responsive PET TeMs-g-PS-g-PMAA membranes were obtained under optimal conditions of UV-initiated controlled RAFT graft polymerization of PMAA onto the hydrophobic PET TeMs-g-PS surface: PMAA concentration of 117 mM, RAFT agent-to-initiator molar ratio of 1:10, irradiation time of 60 min, and a UV-source distance of 10 cm. Under these conditions, the DG_{PMAA} reached 1.1±0.06%, and the membrane surface exhibited a pronounced pH response: at pH 9, the CA was 65°, while at pH 2, it increased to 90°. The resulting membranes had an average pore diameter of 2.01±0.03 μm.

 doi:10.20944/preprints202506.2325.v1

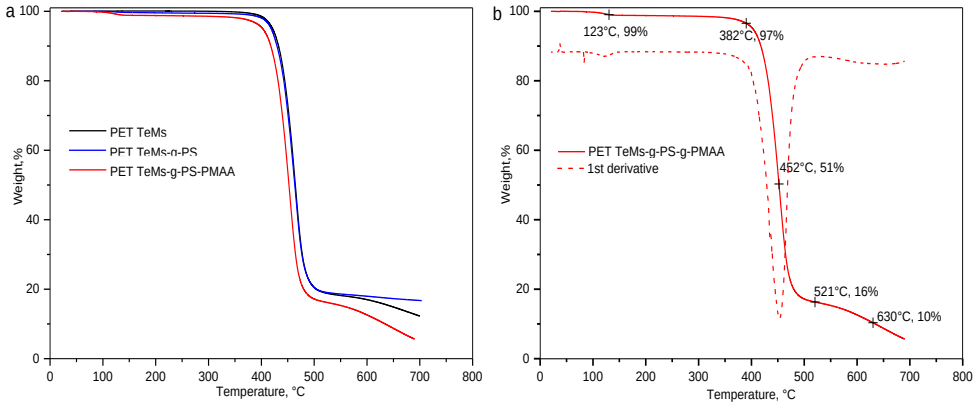

Figure 6. TGA thermograms (a) of PET TeMs, PET TeMs-g-PS, and PET TeMs-g-PS-g-PMAA, TGA and corresponding DTG curves (b) of PET TeMs-g-PS-g-PMAA.

PMAA grafting is confirmed by FTIR-ATR spectroscopy, where the spectra after modification exhibit absorption bands characteristic of aliphatic CH groups of PMAA (2852 and 2925 cm^{-1}), along with a decrease in the intensity of PET and PS peaks. Thermogravimetric analysis reveals an additional mass loss at 123°C, attributed to the evaporation of adsorbed volatile components, and a shift in the main decomposition process to 452°C, with a 51% mass loss, indicating PMAA chain degradation. AFM and SEM analyses reveal an increase in surface roughness and the formation of a denser and more uniform morphology as DG_{PMAA} increases, which is also accompanied by changes in surface mechanical properties.

The obtained PET TeMs-g-PS-g-PMAA were tested for the separation of direct and reverse two-component WOE. For the separation of "oil-in-water" emulsions, the membrane was converted to a hydrophilic state by pre-soaking for 30 min in pH 9, allowing water to pass freely through the pores while oil droplets were retained. Conversely, for reverse "water-in-oil" emulsions, the membrane was made hydrophobic (pH 2), enabling the oil phase to pass through while dispersed water droplets were retained. Figure 7 shows the flux dynamics of PET TeMs-g-PS-g-PMAA over 5 separation cycles of various emulsion types at vacuum pressures of 500, 700, and 900 mbar. Table 2 summarizes the quantitative parameters for the first cycle at 900 mbar: flux (F, L m^{-2} h^{-1}), flux recovery ratio (FR, %), total flux reduction ratio (TR, %), separation efficiency over 5 cycles (R, %), and comparison with other studies.

F gradually decreases over 5 cycles for all types of WOE. For direct emulsions, PET TeMs-g-PS-g-PMAA shows high initial F and over 90% of the oil phase is separated from water. For example, at 900 mbar, the initial F for the chloroform-in-water emulsion was 370 L m^{-2} h^{-1} with a separation efficiency of 90%. For less volatile and more viscous oils, F is lower: for o-xylene-in-water — 190 L m^{-2} h^{-1} and R 98%, for cetane-in-water — 70 L m^{-2} h^{-1} and R 93%.

Table 2. Main quantitative separation parameters for direct and reverse emulsions using PET TeMs-g-PS-g-PMAA, compared with literature data.

Material	Property	Emulsion	Pressure	F, L m^{-2} h^{-1}	R, %	FR, %	TR, %	Ref.
PET TeMs-g-PS-g-PMAA	Hydrophilicity pH>pKa_{PMAA}	Chloroform-in-water	900 mbar	370	90	88	2	This work
			700 mbar	410	92	-	-	
			500 mbar	460	93	-	-	
		o-Xylene-in-water	900 mbar	195	98	69	52	
			700 mbar	290	98		-	
			500 mbar	420	99		-	
		Cetane-in-water	900 mbar	70	93	54	64	
			700 mbar	135	90		-	

 doi:10.20944/preprints202506.2325.v1

			500 mbar	150	95		-	
	Hydrophobicity pH<pKa$_{PMAA}$	Water-in-chloroform	900 mbar	330	85	91	25	
			700 mbar	420	92		-	
			500 mbar	810	96		-	
		Water-in-*o*-xylene	900 mbar	170	92	81	19	
			700 mbar	310	92			
			500 mbar	485	88			
		Water-in-cetane	900 mbar	70	99	70	10	
			700 mbar	80	94			
			500 mbar	650	93			
PET TeMs-g-PS-g-PAA	Hydrophilicity pH>pKa$_{PAA}$	Chloroform-in-water	900 mbar	2500	94±5	82	22	[30]
	Hydrophobicity pH<pKa$_{PAA}$	Water-in-chloroform	900 mbar	1400	97±1	96	46	
Ti2SnC-MAX-PES	Hydrophilicity	Oil-in-water	0.3 kPa	355	80	65	-	[49]
MIL88A@TA@APTES-PVDF	Superhydrophilicity	Oil-in-water	Gravity	2600	99	94	-	[50]
PAN@Co-MOF	Superoleophobicity, water wetting	Cyclohexane-in-water	2-8 kPa	1600	99	-	-	[51]
	Superhydrophobi-city, oil wetting	Water-in-cyclohexane	2-8 kPa	1040	99	-	-	
M-PD/HPA@PVDF	Hydrophilicity	Hexane-in-water	0.3 kPa	150	99	83	37	[52]

Lowering the pressure from 900 to 700 and 500 mbar increases vacuum, and F significantly rises in the first cycle. For chloroform-in-water, F increased from 370 to 410 L m^{-2} h^{-1}, for o-xylene-in-water — from 195 to 460 L m^{-2} h^{-1}, and for cetane-in-water — from 70 to 150 L m^{-2} h^{-1}. However, higher vacuum leads to a more pronounced F drop over cycles. For chloroform-in-water at 900 mbar, F decreased to 80 L m^{-2} h^{-1}, and at 500 mbar — to 190 L m^{-2} h^{-1}. A similar trend was observed for other emulsion types. Stable F over 5 cycles was noted for cetane-in-water. At low vacuum (900 mbar), F slightly decreased from 70 to 60 L m^{-2} h^{-1}. Increasing vacuum to 700 and 500 mbar led to a drop from 135 to 65 L m^{-2} h^{-1} and from 150 to 50 L m^{-2} h^{-1}, respectively. This indicates that for direct emulsions, the membrane shows better stability under lower vacuum, despite a lower initial F.

F for reverse emulsions (Figure 7b,d,f) decreased more sharply than for direct emulsions (Figure 7a,c,e), indicating surface and pore fouling by organic components. At 900 mbar, F for water-in-chloroform dropped from 330 to 17 L m^{-2} h^{-1}, for water-in-o-xylene — from 170 to 20 L m^{-2} h^{-1}, and for water-in-cetane — from 70 to 10 L m^{-2} h^{-1}. Under stronger vacuum, F in the first cycle was even higher compared to direct emulsions. For water-in-chloroform at 500 mbar, F was 810 L m^{-2} h^{-1}, at 700 mbar — 420 L m^{-2} h^{-1}, at 900 mbar — 330 L m^{-2} h^{-1}. However, in all cases F dropped sharply by cycles 3–5: down to 40, 20, and 17 L m^{-2} h^{-1}, respectively. A similar pattern was seen for water-in-o-xylene, where F dropped to 40–20 L m^{-2} h^{-1} by cycle 5. The lowest fluxes were observed for water-in-cetane: at 500 mbar — from 650 to 20 L m^{-2} h^{-1}, at 700 mbar — from 80 to 10 L m^{-2} h^{-1}, and at 900 mbar — from 70 to 10 L m^{-2} h^{-1}. Moreover, at 500 mbar in cycles 4–5, water leakage through the membrane was detected, and R for water-in-cetane dropped to 91–92%, while in other modes it exceeded 95%. Despite the sharp F decrease for reverse emulsions, separation efficiency remained high at 85–99%.

 doi:10.20944/preprints202506.2325.v1

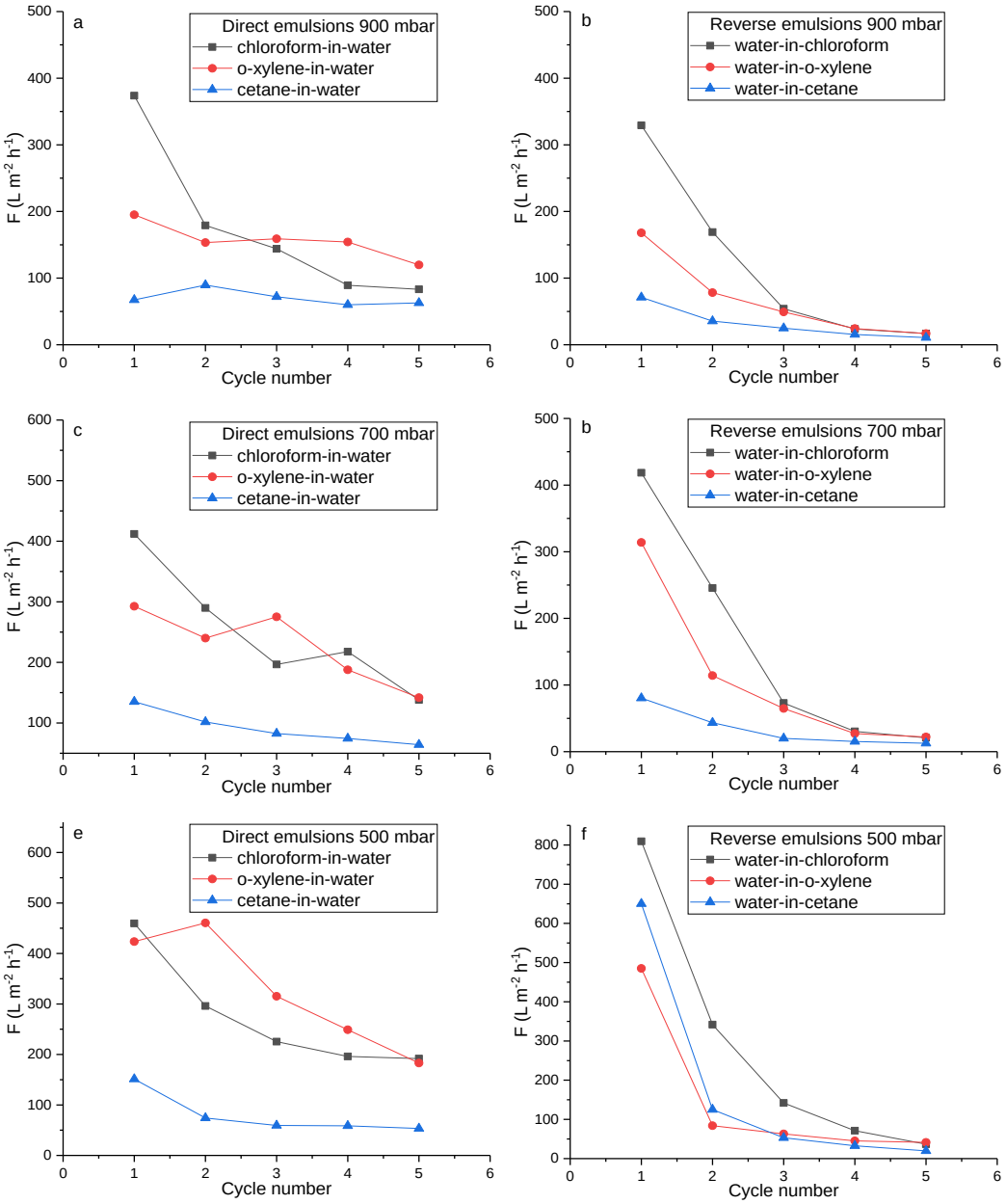

Figure 7. F variation during five separation cycles of direct (a, c, e) and reverse (b, d, f) emulsions at 900 mbar (a, b), 700 mbar (c, d), and 500 mbar (e, f) using PET TeMs-g-PS-g-PMAA.

Thus, PET TeMs-g-PS-g-PMAA shows more stable hydrophilicity than hydrophobicity, confirmed by more stable F over 5 separation cycles and by more pronounced organic fouling in the hydrophobic mode. Additionally, for chloroform-in-water, FR was 85% and TR was 2%, indicating 85% recovery of initial F and very low irreversible fouling (2%). For water-in-chloroform, initial F was recovered at 91%, but irreversible fouling reached 25%. This difference is due to the fouling nature: in hydrophilic mode, oil droplets are weakly adsorbed and easily washed away, while in hydrophobic mode, organic components deposit firmly in the pores and are harder to remove.

Comparison with PET TeMs-g-PS-g-PAA shows that using poly(acrylic acid) (PAA) enables a more efficient transition to the hydrophobic state than PMAA. For PET TeMs-g-PS-g-PAA at pH 2, a higher F of 1400 L m^{-2} h^{-1} was achieved. This is due to the better ability of PAA to collapse at low pH, while PMAA forms less compact coils due to conformational hindrance[44,47] and overlaps the PS layer. This confirms that the choice of polar block significantly affects wettability switching efficiency. PET TeMs-g-PS-g-PMAA, in terms of key parameters, is comparable and even superior to M-

 doi:10.20944/preprints202506.2325.v1

PD/HPA@PVDF and Ti_2SnC-MAX-PES in antifouling and separation performance, but slightly inferior to superhydrophilic and superhydrophobic MIL88A@TA@APTES-PVDF and PAN@Co-MOF. Despite the lower flux compared to some high-performance superhydrophilic membranes, PET TeMs-g-PS-g-PMAA provides stable F in direct emulsion separation, maintains high R (85–99%), and exhibits effective antifouling properties in both hydrophilic (chloroform-in-water, TR 2%) and hydrophobic (water-in-cetane, TR 10%) configurations. The versatility toward emulsion type and controllable wettability make these membranes promising for applications requiring switchable separation modes.

4. Conclusions

As a result of UV-initiated RAFT graft polymerization of MAA onto the surface of PET TeMs-g-PS, pH-responsive membranes PET TeMs-g-PS-g-PMAA were obtained. The optimized grafting conditions (117 mM PMAA, RAFT:initiator 1:10, 60 min, 10 cm from UV source) provided DG_{PMAA} of 1.1%, pH response CA 65° (pH 9) – 90° (pH 2), and a pore diameter of 2.01 μm.

The grafting of PMAA is confirmed by several analytical methods. New bands appear in the FTIR spectra at 2852 and 2925 cm^{-1}, characteristic of CH-group vibrations of PMAA. TGA shows additional thermal decomposition stages at 521°C and 630°C, and the main degradation peak shifts from 463°C to 452°C, indicating the presence of the grafted polymer. SEM reveals smoothing of the surface morphology and pore narrowing. AFM detects an increase in surface roughness Ra and Rq from 8.4 nm and 12 nm (PET TeMs-g-PS) to 17 and 24 nm, respectively. TB sorption results show an increase in the content of carboxyl groups from 0.8 to 1.16 mmol/L.

PET TeMs-g-PS-g-PMAA demonstrate high efficiency in the separation of direct emulsions: stable F over 5 cycles, separation efficiency of 90–98%, and low irreversible fouling (TR up to 2% for "chloroform-in-water"). In reverse emulsions, higher initial F values are observed but with a significant decrease already by cycles 3–5, indicating less stable hydrophobicity at low pH.

Thus, despite limited hydrophobic stability, PET TeMs-g-PS-g-PMAA membranes exhibit excellent antifouling properties, high separation efficiency, and versatility due to their pH-responsivity. These membranes can be considered a competitive solution among switchable membrane systems for emulsion separation. Future research prospects are related to improving the membrane stability at low pH and enhancing performance in the hydrophobic state.

Author Contributions: Conceptualization, I.B.M. and I.V.K.; methodology, I.V.K., I.B.M. and D.D.O.; validation, N.Zh. and N.A.; formal analysis, N.Zh., N.A. and D.D.O.; investigation, I.B.M., D.D.O. and N.Zh.; data curation, I.B.M. and D.D.O.; writing—original draft preparation, I.B.M.; writing—review and editing, I.V.K. and Zh.K.Zh.; supervision, I.B.M. and I.V.K.; project administration, I.B.M.; funding acquisition, I.B.M. All authors have read and agreed to the published version of the manuscript.

Funding: This research was funded by the Science Committee of the Ministry of Science and Higher Education of the Republic of Kazakhstan, Grant No. AP27511347, and partially by the Project "Young Scientist", Grant No. AP14972816. The APC was funded by Grant No. AP27511347.

Data Availability Statement: The data presented in this study are available on request from the corresponding author.

Conflicts of Interest: The authors declare no conflict of interest.

Acknowledgments: In preparing this manuscript, the authors utilized ChatGPT-4o to enhance the English grammar and style for improved clarity and readability. The original draft and subsequent revisions were written by the authors themselves. Following the use of these tools, the authors thoroughly reviewed and edited the output and assume full responsibility for the final content of this publication.

 doi:10.20944/preprints202506.2325.v1

References

1. Zhang, N.; Yang, X.; Wang, Y.; Qi, Y.; Zhang, Y.; Luo, J.; Cui, P.; Jiang, W. A Review on Oil/Water Emulsion Separation Membrane Material. *J Environ Chem Eng* **2022**, *10*, 107257, doi:10.1016/J.JECE.2022.107257.
2. Zhang, N.; Yang, X.; Wang, Y.; Qi, Y.; Zhang, Y.; Luo, J.; Cui, P.; Jiang, W. A Review on Oil/Water Emulsion Separation Membrane Material. *J Environ Chem Eng* **2022**, *10*, 107257, doi:10.1016/J.JECE.2022.107257.
3. Liu, X.; Zhang, G.; Al Mohawes, K.B.; Khashab, N.M. Smart Membranes for Separation and Sensing. *Chem Sci* **2024**, *15*, 18772–18788, doi:10.1039/D4SC04793A.
4. Karunakar, K.K.; Cheriyan, B.V.; Anandakumar, R.; Murugathirumal, A.; Senthilkumar, A.; Nandhini, J.; Kataria, K.; Yabase, L. Stimuli-Responsive Smart Materials: Bridging the Gap between Biotechnology and Regenerative Medicine. *Bioprinting* **2025**, *48*, e00415, doi:10.1016/J.BPRINT.2025.E00415.
5. Rehman, A.; Sohail, M.; Baig, N.; Yuan, K.; Abdala, A.; Wahab, M.A. Next-Generation Stimuli-Responsive Smart Membranes: Developments in Oil/Water Separation. *Adv Colloid Interface Sci* **2025**, *341*, 103487, doi:10.1016/J.CIS.2025.103487.
6. Gao, Z.; Dong, Y.; Huang, C.; Hussain Abdalkarim, S.Y.; Yu, H.Y.; Tam, K.C. On-Demand plus and Minus Strategy to Design Conductive Nanocellulose: From Low-Dimensional Structural Materials to Multi-Dimensional Smart Sensors. *Chemical Engineering Journal* **2025**, *510*, 161552, doi:10.1016/J.CEJ.2025.161552.
7. Korolkov, I. V.; Mashentseva, A.A.; Güven, O.; Gorin, Y.G.; Kozlovskiy, A.L.; Zdorovets, M. V.; Zhidkov, I.S.; Cholach, S.O. Electron/Gamma Radiation-Induced Synthesis and Catalytic Activity of Gold Nanoparticles Supported on Track-Etched Poly(Ethylene Terephthalate) Membranes. *Mater Chem Phys* **2018**, *217*, 31–39, doi:10.1016/J.MATCHEMPHYS.2018.06.039.
8. Chakarvarti, S.K. Track-Etch Membranes Enabled Nano-/Microtechnology: A Review. *Radiat Meas* **2009**, *44*, 1085–1092, doi:10.1016/J.RADMEAS.2009.10.028.
9. Barsbay, M.; Güven, O. Grafting in Confined Spaces: Functionalization of Nanochannels of Track-Etched Membranes. *Radiation Physics and Chemistry* **2014**, *105*, 26–30, doi:10.1016/J.RADPHYSCHEM.2014.05.018.
10. Hadi, M.K.; Wang, X.; Peng, Y.; Sangaraju, S.; Ran, F. Functional Polymeric Membrane Materials: A Perspective from Versatile Methods and Modification to Potential Applications. *Polymer Science & Technology* **2024**, doi:10.1021/POLYMSCITECH.4C00030.
11. Semsarilar, M.; Abetz, V.; Semsarilar, M.; Abetz, V. Polymerizations by RAFT: Developments of the Technique and Its Application in the Synthesis of Tailored (Co)Polymers. *Macromol Chem Phys* **2021**, *222*, 2000311, doi:10.1002/MACP.202000311.
12. Rong, L.H.; Caldona, E.B.; Advincula, R.C. PET-RAFT Polymerization under Flow Chemistry and Surface-initiated Reactions. *Polym Int* **2022**, *72*, 145–157, doi:10.1002/PI.6475.
13. Adamson, A.W.; Klerer, J. Modification of Pet Surfaces with End-Functionalized Polymers Prepared from Raft Agents to Achieve Antibacterial Properties = Modifikasi Permukaan Pet Dengan Polimer-Polimer Fungsional Dari Agen Raft Untuk Mencapai Sifat Antibakteri. *J Electrochem Soc* **2015**, *124*, 192C-192C, doi:10.1149/1.2133374/PDF.
14. Pan, K.; Ren, R.; Li, H.; Cao, B. Preparation of Dual Stimuli-Responsive PET Track-Etched Membrane by Grafting Copolymer Using ATRP. *Polym Adv Technol* **2013**, *24*, 22–27, doi:10.1002/PAT.3044.
15. Yeszhanov, A.B.; Korolkov, I.V.; Shakayeva, A.K.; Lissovskaya, L.I.; Zdorovets, M.V. Preparation of Poly(Ethylene Terephthalate) Track-Etched Membranes for the Separation of Water-Oil Emulsions. *Eurasian Journal of Chemistry* **2023**, *2023*, 131–138, doi:10.31489/2959-0663/2-23-5.
16. Tai, S.L.; Abidin, M.N.Z.; Ma'amor, A.; Hashim, N.A.; Hashim, M.L.H. Polyethylene Terephthalate Membrane: A Review of Fabrication Techniques, Separation Processes, and Modifications. *Sep Purif Technol* **2025**, *354*, 129343, doi:10.1016/J.SEPPUR.2024.129343.

17. Mashentseva, A.A.; Khassen, T.G.; Krasnov, V.A.; Zhumazhanova, A.T.; Kassymzhanov, M.T. МОДИФИКАЦИЯ ПОВЕРХНОСТИ ПЭТФ ТРЕКОВЫХ МЕМБРАН ФУНКЦИОНАЛЬНЫМИ МОНОМЕРАМИ ПОД ВОЗДЕЙСТВИЕМ УСКОРЕННЫХ ЭЛЕКТРОНОВ. *Вестник НЯЦ РК* **2020**, *0*, 5–11, doi:10.52676/1729-7885-2020-1-5-11.
18. Parmanbek, N.; Sütekin, S.D.; Barsbay, M.; Aimanova, N.A.; Mashentseva, A.A.; Alimkhanova, A.N.; Zhumabayev, A.M.; Yanevich, A.; Almanov, A.A.; Zdorovets, M. V. Environmentally Friendly Loading of Palladium Nanoparticles on Nanoporous PET Track-Etched Membranes Grafted by Poly(1-Vinyl-2-Pyrrolidone) via RAFT Polymerization for the Photocatalytic Degradation of Metronidazole. *RSC Adv* **2023**, *13*, 18700–18714, doi:10.1039/D3RA03226D.
19. Friebe, A.; Ulbricht, M. Controlled Pore Functionalization of Poly(Ethylene Terephthalate) Track-Etched Membranes via Surface-Initiated Atom Transfer Radical Polymerization. *Langmuir* **2007**, *23*, 10316–10322, doi:10.1021/LA7016962/SUPPL_FILE/LA7016962_SI.PDF.
20. Smolinska, K.; Bryjak, M. Plasma Modified Track-Etched Membranes for Separation of Alkaline Ions. *The Open Access Journal of Science and Technology AgiAl Publishing House* **2014**, *2*, doi:10.11131/2014/101068.
21. Shakayeva, A.K.; Yeszhanov, A.B.; Zhumazhanova, A.T.; Korolkov, I.V.; Zdorovets, M.V. Fabrication of Hydrophobic PET Track-Etched Membranes Using 2,2,3,3,4,4,4-Heptafluorobutyl Methacrylate for Water Desalination by Membrane Distillation. *EURASIAN JOURNAL OF CHEMISTRY* **2024**, *29*, 81–88, doi:10.31489/2959-0663/2-24-5.
22. Shakayeva, A.K.; Yeszhanov, A.B.; Borissenko, A.N.; Kassymzhanov, M.T.; Zhumazhanova, A.T.; Khlebnikov, N.A.; Nurkassimov, A.K.; Zdorovets, M. V.; Güven, O.; Korolkov, I. V. Surface Modification of Polyethylene Terephthalate Track-Etched Membranes by 2,2,3,3,4,4,5,5,6,6,7,7-Dodecafluoroheptyl Acrylate for Application in Water Desalination by Direct Contact Membrane Distillation. *Membranes (Basel)* **2024**, *14*, 145, doi:10.3390/MEMBRANES14070145/S1.
23. Korolkov, I. V.; Kuandykova, A.; Yeszhanov, A.B.; Güven, O.; Gorin, Y.G.; Zdorovets, M. V. Modification of PET Ion-Track Membranes by Silica Nanoparticles for Direct Contact Membrane Distillation of Salt Solutions. *Membranes 2020, Vol. 10, Page 322* **2020**, *10*, 322, doi:10.3390/MEMBRANES10110322.
24. Guo, Z.; Wang, Y.; Liang, Z.; Zhang, Z.; Xie, J.; Gui, X.; Hou, B.; Mo, D.; Lu, L.; Yao, H. Hydrophobic Modified PET Ion Track-Etched Membrane for Oil/Water Separation. *Journal of Water Process Engineering* **2023**, *54*, 103997, doi:10.1016/J.JWPE.2023.103997.
25. Yeszhanov, A.B.; Muslimova, I.B.; Melnikova, G.B.; Petrovskaya, A.S.; Seitbayev, A.S.; Chizhik, S.A.; Zhappar, N.K.; Korolkov, I. V.; Güven, O.; Zdorovets, M. V. Graft Polymerization of Stearyl Methacrylate on PET Track-Etched Membranes for Oil–Water Separation. *Polymers (Basel)* **2022**, *14*, doi:10.3390/POLYM14153015.
26. Dansawad, P.; Yang, Y.; Li, X.; Shang, X.; Li, Y.; Guo, Z.; Qing, Y.; Zhao, S.; You, S.; Li, W. Smart Membranes for Oil/Water Emulsions Separation: A Review. *Advanced Membranes* 2022, *2*.
27. Gupta, R.K.; Dunderdale, G.J.; England, M.W.; Hozumi, A. Oil/Water Separation Techniques: A Review of Recent Progresses and Future Directions. *J Mater Chem A Mater* **2017**, *5*, 16025–16058, doi:10.1039/C7TA02070H.
28. Rasouli, S.; Rezaei, N.; Hamedi, H.; Zendehboudi, S.; Duan, X. Superhydrophobic and Superoleophilic Membranes for Oil-Water Separation Application: A Comprehensive Review. *Mater Des* **2021**, *204*, doi:10.1016/J.MATDES.2021.109599.
29. Wu, H.; Wang, Y.; Mao, X.; Gao, Z.; Luo, S.; Kipper, M.J.; Huang, L.; Tang, J. Recent Advances in Electrospinning Smart Membranes for Oil/Water Separation. *Surfaces and Interfaces* **2024**, *55*, 105427, doi:10.1016/J.SURFIN.2024.105427.

30. Muslimova, I.B.; Zhumanazar, N.; Melnikova, G.B.; Yeszhanov, A.B.; Zhatkanbayeva, Z.K.; Chizhik, S.A.; Zdorovets, M. V.; Güven, O.; Korolkov, I. V. Preparation and Application of Stimuli-Responsive PET TeMs: RAFT Graft Block Copolymerisation of Styrene and Acrylic Acid for the Separation of Water–Oil Emulsions. *RSC Adv* **2024**, *14*, 14425–14437, doi:10.1039/D4RA02117G.
31. Zhou, Y.N.; Li, J.J.; Luo, Z.H. Toward Efficient Water/Oil Separation Material: Effect of Copolymer Composition on PH-Responsive Wettability and Separation Performance. *AIChE Journal* **2016**, *62*, 1758–1771, doi:10.1002/AIC.15145.
32. Yang, J.; Loh, X.J.; Tan, B.H.; Li, Z. PH-Responsive Poly(Dimethylsiloxane) Copolymer Decorated Magnetic Nanoparticles for Remotely Controlled Oil-in-Water Nanoemulsion Separation. *Macromol Rapid Commun* **2019**, *40*, 1800013, doi:10.1002/MARC.201800013.
33. Muslimova, I.B.; Zhatkanbayeva, Z.K.; Omertasov, D.D.; Melnikova, G.B.; Yeszhanov, A.B.; Güven, O.; Chizhik, S.A.; Zdorovets, M. V.; Korolkov, I. V. Stimuli-Responsive Track-Etched Membranes for Separation of Water–Oil Emulsions. *Membranes (Basel)* **2023**, *13*, 523, doi:10.3390/MEMBRANES13050523/S1.
34. Ma, H.; Cameron, A. Dual-Responsive Polymers Synthesized via RAFT Polymerization for Controlled Demulsification and Desorption. *Journal of Polymer Research* **2023**, doi:10.21203/RS.3.RS-2811667/V1.
35. Chen, J.; Yu, Q.; Wang, M.; Liu, D.; Dong, L.; Cui, Z.; He, B.; Li, J.; Yan, F. Superhydrophilic/Underwater Superoleophobic PVDF Ultrafiltration Membrane with PH-Responsive Self-Cleaning Performance for Efficient Oil-Water Separation. *Sep Purif Technol* **2024**, *330*, 125420, doi:10.1016/J.SEPPUR.2023.125420.
36. Chen, Q.; Deng, X.; An, Z. PH-Induced Inversion of Water-in-Oil Emulsions to Oil-in-Water High Internal Phase Emulsions (HIPEs) Using Core Cross-Linked Star (CCS) Polymer as Interfacial Stabilizer. *Macromol Rapid Commun* **2014**, *35*, 1148–1152, doi:10.1002/MARC.201400085.
37. Yeszhanov, A.B.; Korolkov, I. V; Dosmagambetova, S.S.; Zdorovets, M. V; Güven, O. Recent Progress in the Membrane Distillation and Impact of Track-Etched Membranes. **2021**, doi:10.3390/polym.
38. Korolkov, I. V.; Narmukhamedova, A.R.; Melnikova, G.B.; Muslimova, I.B.; Yeszhanov, A.B.; Zhatkanbayeva, Z.K.; Chizhik, S.A.; Zdorovets, M. V. Preparation of Hydrophobic PET Track-Etched Membranes for Separation of Oil–Water Emulsion. *Membranes (Basel)* **2021**, *11*, doi:10.3390/MEMBRANES11080637.
39. Guerre, M.; Wahidur Rahaman, S.M.; Améduri, B.; Poli, R.; Ladmiral, V. RAFT Synthesis of Well-Defined PVDF-b-PVAc Block Copolymers. *Polym Chem* **2016**, *7*, 6918–6933, doi:10.1039/C6PY01247G.
40. Keddie, D.J. A Guide to the Synthesis of Block Copolymers Using Reversible-Addition Fragmentation Chain Transfer (RAFT) Polymerization. *Chem Soc Rev* **2014**, *43*, 496–505, doi:10.1039/C3CS60290G.
41. Monteiro, M.J. Modeling the Molecular Weight Distribution of Block Copolymer Formation in a Reversible Addition-Fragmentation Chain Transfer Mediated Living Radical Polymerization. *J Polym Sci A Polym Chem* **2005**, *43*, 5643–5651, doi:10.1002/POLA.21069.
42. Shu, H.; Wang, C.; Yang, L.; Sun, D.; Song, C.; Zhang, X.; Chen, D.; Ma, Y.; Yang, W. Preparation of Multifunctional PET Membrane and Its Application in High-Efficiency Filtration and Separation in Complex Environment. *J Hazard Mater* **2024**, *474*, 134669, doi:10.1016/J.JHAZMAT.2024.134669.
43. Shi, Q.; Su, Y.; Ning, X.; Chen, W.; Peng, J.; Jiang, Z. Graft Polymerization of Methacrylic Acid onto Polyethersulfone for Potential PH-Responsive Membrane Materials. *J Memb Sci* **2010**, *347*, 62–68, doi:10.1016/J.MEMSCI.2009.10.006.
44. Romero-Fierro, D.A.; Camacho-Cruz, L.A.; Bustamante-Torres, M.R.; Hidalgo-Bonilla, S.P.; Bucio, E. Modification of Cotton Gauzes with Poly(Acrylic Acid) and Poly(Methacrylic Acid) Using Gamma

 doi:10.20944/preprints202506.2325.v1

Radiation for Drug Loading Studies. *Radiation Physics and Chemistry* **2022**, *190*, doi:10.1016/j.radphyschem.2021.109787.

45. Henkel, R.C. Der Einfluss Der UV-Initiierten RAFT-Polymerisation Auf Die Strukturen Und Eigenschaften von Polymernetzwerken. **2014**, doi:10.53846/GOEDISS-4701.
46. Han, S.; Wu, J.; Zhang, Y.; Lai, J.; Chen, Y.; Zhang, L.; Tan, J. Utilization of Poor RAFT Control in Heterogeneous RAFT Polymerization. *Macromolecules* **2021**, *54*, 4669–4681, doi:10.1021/ACS.MACROMOL.1C00381/SUPPL_FILE/MA1C00381_SI_001.PDF.
47. Hu, Y.; Hou, Q.; Liu, H.; Ye, X. One-Pot, Surfactant-Free Synthesis of Poly(Styrene-N,N′-Methylenebis(2-Propenamide)-Acrylic Acid) and Poly(Styrene-N,N′-Methylenebis(2-Propenamide)-Methacrylic Acid) Microspheres for Adsorptive Removal of Heavy Metal Ions. *Colloids Surf A Physicochem Eng Asp* **2024**, *683*, doi:10.1016/j.colsurfa.2023.132951.
48. Korolkov, I. V.; Yeszhanov, A.B.; Zdorovets, M. V.; Gorin, Y.G.; Güven, O.; Dosmagambetova, S.S.; Khlebnikov, N.A.; Serkov, K. V.; Krasnopyorova, M. V.; Milts, O.S.; et al. Modification of PET Ion Track Membranes for Membrane Distillation of Low-Level Liquid Radioactive Wastes and Salt Solutions. *Sep Purif Technol* **2019**, *227*, doi:10.1016/j.seppur.2019.115694.
49. Safarpour, M.; Hosseinpour, S.; Haddad Irani-nezhad, M.; Orooji, Y.; Khataee, A. Fabrication of Ti2SnC-MAX Phase Blended PES Membranes with Improved Hydrophilicity and Antifouling Properties for Oil/Water Separation. *Molecules* **2022**, *27*, doi:10.3390/molecules27248914.
50. Feng, L.; Gao, Y.; Yin, W.; Gao, B.; Yue, Q. Multi-Functional Membrane with Double-Barrier and Self-Cleaning Ability for Emulsion Separation: Fouling Model and Long-Term Operation. *J Memb Sci* **2024**, *696*, doi:10.1016/j.memsci.2024.122466.
51. Liu, Y.; Wang, Y.; Zhang, T.C.; Ouyang, L.; Yuan, S. Switchable Superlyophobic PAN@Co-MOF Membrane for on-Demand Emulsion Separation and Efficient Soluble Dye Degradation. *Sep Purif Technol* **2024**, *331*, doi:10.1016/j.seppur.2023.125730.
52. Li, D.; Lin, J.; An, Z.; Li, Y.; Zhu, X.; Yang, J.; Wang, Q.; Zhao, J.; Zhao, Y.; Chen, L. Enhancing Hydrophilicity and Comprehensive Antifouling Properties of Microfiltration Membrane by Novel Hyperbranched Poly(N-Acryoyl Morpholine) Coating for Oil-in-Water Emulsion Separation. *React Funct Polym* **2020**, *156*, doi:10.1016/j.reactfunctpolym.2020.104735.